# Finding Image Distributions on Active Curves

Ismail Ben Ayed[1,2], Amar Mitiche[3], Mohamed Ben Salah[3], and Shuo Li[1,2]
[1]GE Healthcare, London, ON, Canada
[2] University of Western Ontario, London, ON, Canada
[3] Institut National de la Recherche Scientifique, INRS-EMT, Montreal, QC, Canada

## Abstract

*This study investigates an active curve functional which measures a similarity between the distribution of an image feature on the curve and a model distribution learned* a priori*. The curve evolution equation resulting from the minimization of this contour-based functional can be viewed as a geodesic active contour with a* variable stopping function*. The variable stopping function depends on the distribution of image feature on the curve and, therefore, can deal with difficult cases where the desired boundary corresponds to very weak image transitions. We ran several experiments supported by quantitative performance evaluations over several examples of segmentation and tracking of the left ventricle inner and outer boundaries in cardiac magnetic resonance image sequences. The results are significantly more accurate than with region-based and edge-based functionals.*

## 1. Introduction

Image segmentation is a fundamental problem in computer vision and image processing. It serves important useful applications in diverse fields such as robotics, remote sensing, surveillance, and medical image analysis. Amenable to the introduction of various types of constraints on the segmentation, the level set active curve framework has resulted in the most effective algorithms [1]–[14]. The formalism yields a curve evolution equation following the minimization of a functional. Some of the algorithms are *region-based* [1]–[6], where statistics of the image within the segmentation regions guide the curve evolution, and others are *edge-based* [7]–[14], where the evolution is guided by the image data on the active curve.

In statistical, region-based algorithms, each segmentation region is characterized by an image distribution, i.e., the regions are assumed to differ by their image statistics. Following the work of Chan and Vese [1], which uses the regions means, various region-based algorithms have been developed [2]-[6]. The most effective use nonparametric distributions and regions models learned *a priori* from training images [3], [4], [5]. For instance, in [3], curve evolution seeks a region whose sample distribution most closely matches a learned model. In [4], the authors use prior information about the overlap between the image distributions within the segmentation regions to improve the results. Although effective in many cases, region-based data terms and priors may not be sufficient to recover the desired segmentation in important, difficult situations where different regions in the image have the same image statistics. This occurs frequently in medical image segmentation. Fig. 1 depicts a typical instance, where parts of the foreground and background regions in a cardiac image have approximately the same intensity profile. In this case, the region-based energies in [3], [4], [5] cannot recover accurately the target segmentation. Therefore, further relevant information on the boundary of interest is necessary.

Edge-based algorithms generally attract an active curve $\Gamma(s) : [0,1] \rightarrow \Omega$ toward high transitions (significant edges) of the image $\mathbf{I} : \Omega \subset \mathbb{R}^2 \rightarrow \mathbb{R}$ by minimizing a *geodesic integral* having the following general form [8], [9], [10], [11], [12]

$$\int_{\Gamma} g(\mathbf{I}) ds, \tag{1}$$

where $g$ is an edge indicator function which depends solely on image data, not on the curve. A common choice of $g$, often referred to as a *stopping function*, is a monotonically decreasing function of the image gradient, for instance

$$g(\mathbf{I}) = \frac{1}{1 + \|\nabla \mathbf{I}\|^p}, p = 1, 2 \tag{2}$$

The curve flow minimizing this geodesic integral is known as the geodesic active contour (GAC) [8]. Although effective in various cases, the GAC cannot deal with the difficult situations where parts of the desired boundary correspond to very weak image transitions, i.e., where the norm of image gradient is null or nearly null (cf. the typical example in Fig. 1 (e)).

The purpose of this study is to take full advantage of the statistical image information that one can learn about the

978-1-4244-6985-7/10/$26.00 ©2010 IEEE 

boundary of interest. We propose to minimize an original contour-based functional which measures a similarity between the distribution of an image feature on the curve (or in a narrow band around the curve) and a model distribution learned *a priori*. We are currently using the Bhattacharyya coefficient as a similarity measure, and the image or image gradient as feature, although other features can be used. Minimization of the proposed functional, via the Euler-Lagrange equation and level set implementation, results in a curve evolution equation which can be interpreted as a GAC with a *variable* stopping function. The stopping function in this equation has two fundamental differences with the standard GAC stopping function. First, it is a function of the curve, whereas the GAC function is a scalar function that depends solely on the image, not on the curve. Second, it references *global information*, namely the distribution of the image feature on the curve, rather than only pixel-wise image information. Compared to the region-based formulations [3], [4], [6], the proposed functional is fundamentally different because it is contour-based. The marginal similarity with these works is in using the Bhattacharyya measure, but the curve evolution equation we obtained is quite different. As we will see in the experiments, the proposed evolution equation can lead to significant improvements over region-based methods in difficult situations where parts of the target boundary correspond to weak transitions of image data (cf. the typical example in Fig. 1).

We applied the proposed curve evolution to the segmentation and tracking of the left ventricle (LV) inner (endocardium) and outer (epicardium) boundaries in 2D cardiac magnetic resonance (MR) images. We show examples which show clearly the advantage of the proposed functional, and how it can lead to significant improvements in accuracy over existing region-based and edge-based functionals. Our experiments are supported by quantitative performance evaluations in comparisons to independent expert manual segmentations.

## 2. Formulation

### 2.1. Proposed contour-based energy

Let $\mathbf{F_x} = \mathbf{F}(\mathbf{x}) : \Omega \subset \mathbb{R}^2 \rightarrow \mathcal{F}$ be an image feature function defined from the domain $\Omega$ to the feature space $\mathcal{F}$. $\mathbf{F}$ can be the image data such as intensity, the image gradient, or the convolution of the image with an *a priori* specified filter. Let $\Gamma(s) : [0,1] \rightarrow \Omega$ be a simple closed planar parametric curve. Our purpose is to evolve $\Gamma$ following the minimization of an original *contour-based* energy, which measures the similarity between the sample distribution of image feature on the curve and a model learned *a priori*. To introduce our energy as a function of $\Gamma$, let us first consider the following definitions:

- $\mathbf{P}_\Gamma$ is the nonparametric (kernel-based) estimate of the distribution of the image feature on the active curve

$$\forall f \in \mathcal{F} \quad \mathbf{P}_\Gamma(f) = \frac{\oint_\Gamma K(f - \mathbf{F}_{\Gamma(s)})ds}{\mathcal{L}_\Gamma}, \tag{3}$$

where $\mathcal{L}_\Gamma$ is the length of the curve

$$\mathcal{L}_\Gamma = \oint_\Gamma ds \tag{4}$$

Typical choices of $K$ are the Dirac function and the Gaussian kernel ($h$ is the kernel width)

$$K(y) = \frac{1}{\sqrt{2\pi h^2}} exp^{-\frac{y^2}{2h^2}} \tag{5}$$

- $\mathbf{B}$ is the Bhattacharyya coefficient[1] measuring the similarity between two distributions $\mathbf{P}$ and $\mathbf{Q}$ defined over the same feature space $\mathcal{F}$

$$\mathbf{B}(\mathbf{P}, \mathbf{Q}) = \sum_{f \in \mathcal{F}} \sqrt{\mathbf{P}(f)\mathbf{Q}(f)} \tag{6}$$

We assume that the image feature on the boundary of the target region, or within a narrow band around the boundary, is characterized by a model distribution, $\mathcal{M}$, which can be learned *priori*. We propose to minimize the following edge-based energy with respect to $\Gamma$

$$\mathcal{B}(\Gamma) = -\mathbf{B}(\mathbf{P}_\Gamma, \mathcal{M}) \tag{7}$$

Minimizing $\mathcal{B}(\Gamma)$ amounts to finding a curve so that the distribution of the image feature in the neighborhood of the curve most closely matches the model distribution $\mathcal{M}$. Note that other measures of similarity between distributions can be used, for instance the KullbackLeibler divergence. This would change the final evolution equation, but would not change the method conceptually.

### 2.2. Curve evolution minimization equation

The curve evolution equation is obtained by minimizing $\mathcal{B}(\Gamma)$ with respect to $\Gamma$. To this end, we derive the Euler-Lagrange gradient descent equation by embedding curve $\Gamma$ in a one-parameter family of curves: $\Gamma(s,t) : [0,1] \times \mathbb{R}^+ \rightarrow \Omega$, and solving the partial differential descent equation

$$\frac{\partial \Gamma}{\partial t} = -\frac{\partial \mathcal{B}}{\partial \Gamma} \tag{8}$$

where $t$ is an artificial time parameterizing the descent direction, and $\frac{\partial \mathcal{B}}{\partial \Gamma}$ denotes the functional derivative of $\mathcal{B}$ with respect to $\Gamma$. To derive the curve evolution equation, we need to compute the functional derivative in (8). We have:

$$\frac{\partial \mathcal{B}}{\partial \Gamma} = -\frac{1}{2} \sum_{f \in \mathcal{F}} \sqrt{\frac{\mathcal{M}(f)}{\mathbf{P}_\Gamma(f)}} \frac{\partial \mathbf{P}_\Gamma(f)}{\partial \Gamma} \tag{9}$$

[1] The values of $\mathbf{B}$ are always in $[0,1]$, where 0 indicates maximum discrepancy between the distributions, and 1 indicates a perfect match.

Now we need to compute $\frac{\partial \mathbf{P}_\Gamma(f)}{\partial \Gamma}$. We have

$$\frac{\partial \mathbf{P}_\Gamma(f)}{\partial \Gamma} = \frac{\mathcal{L}_\Gamma \frac{\partial \oint_\Gamma K(f-\mathbf{F}_{\Gamma(s)})ds}{\partial \Gamma} - \frac{\partial \mathcal{L}_\Gamma}{\partial \Gamma} \oint_\Gamma K(f-\mathbf{F}_{\Gamma(s)})ds}{\mathcal{L}_\Gamma^2} \tag{10}$$

To compute the derivatives in the right-hand side of equation (9), we consider the following proposition.

**Proposition 1** *For a curve $\Gamma$ and a scalar function $h : \Omega \rightarrow \mathbb{R}$ independent from $\Gamma$, the functional derivative with respect to $\Gamma$ of the integral of $h$ over the curve is given by ($s$ and $t$ are omitted as arguments for simplicity)*

$$\frac{\partial \oint_\Gamma h ds}{\partial \Gamma} = (-h\kappa + < \nabla h, \vec{n} >)\vec{n}$$

*where $\vec{n}$ is the inward unit normal to $\Gamma$ and $\kappa$ the mean curvature function of $\Gamma$.*

The derivative of the above integral, referred to as *geodesic integral*, is well known in the literature [2] , and can be obtained the Euler-Lagrange equations [8].

Applying this result to $\oint_\Gamma K(f-\mathbf{F}_{\Gamma(s)})ds$ and $\mathcal{L}_\Gamma$ in the numerator in (10), and after some algebraic manipulations, we obtain the following functional derivative of $\mathbf{P}_\Gamma(f)$

$$\begin{aligned} \forall f \in \mathcal{F} \ \frac{\partial \mathbf{P}_\Gamma(f)}{\partial \Gamma} &= \frac{1}{\mathcal{L}_\Gamma}\{-K(f-\mathbf{F}_\Gamma)\kappa \\ &+ < \nabla K(f-\mathbf{F}_\Gamma), \vec{n} > \\ &+ \mathbf{P}_\Gamma(f)\kappa\}\vec{n} \end{aligned} \tag{11}$$

Embedding this result in (10), and after some algebraic manipulations, we obtain the following evolution equation minimizing $\mathcal{B}$ ($s$ and $t$ are omitted as arguments of $\Gamma$):

$$\begin{aligned} \frac{\partial \Gamma}{\partial t} &= \frac{1}{2\mathcal{L}_\Gamma}\{\underbrace{(\mathbf{B}(\mathbf{P}_\Gamma, \mathcal{M}) - \sum_{f\in\mathcal{F}} \sqrt{\frac{\mathcal{M}(f)}{\mathbf{P}_\Gamma(f)}} K(f-\mathbf{F}_\Gamma))\kappa}_{Stopping\ force} \\ &- \underbrace{< \nabla \sum_{f\in\mathcal{F}} \sqrt{\frac{\mathcal{M}(f)}{\mathbf{P}_\Gamma(f)}} K(f-\mathbf{F}_\Gamma), \vec{n} >\}\vec{n}}_{Refinement force} \end{aligned} \tag{12}$$

**Connection with the classical geodesic active contour (GAC):** The obtained flow can be viewed as a geodesic active contour with a variable stopping function. Since $\mathbf{B}(\mathbf{P}_\Gamma, \mathcal{M})$ is independent from pixel location, $\nabla \mathbf{B}(\mathbf{P}_\Gamma, \mathcal{M}) = 0$. By adding this gradient we can rewrite the obtained flow in a form similar to the geodesic active contour flow

$$\frac{\partial \Gamma}{\partial t} = \left( \underbrace{\mathcal{G}(\mathbf{P}_\Gamma, \mathcal{M}, \mathbf{F}_\Gamma)\kappa}_{Stopping} - \underbrace{< \nabla \mathcal{G}(\mathbf{P}_\Gamma, \mathcal{M}, \mathbf{F}_\Gamma), \vec{n} >}_{refinement} \right) \vec{n} \tag{13}$$

[2] Recall that the classical geodesic active contour energy corresponds to the integral of $h$, $h = g(\mathbf{F}) = \frac{1}{1+\|\nabla \mathbf{F}\|^p}$, with $p = 1, 2$ and $\mathbf{F}$ is image data

where the stopping function is given in our case by

$$\mathcal{G}(\mathbf{P}_\Gamma, \mathcal{M}, \mathbf{F}_\Gamma) = \mathbf{B}(\mathbf{P}_\Gamma, \mathcal{M}) - \sum_{f\in\mathcal{F}} \sqrt{\frac{\mathcal{M}(f)}{\mathbf{P}_\Gamma(f)}} K(f-\mathbf{F}_\Gamma) \tag{14}$$

$\mathcal{G}(\mathbf{P}_\Gamma, \mathcal{M}, F)$ has two fundamental differences with the GAC stopping function. First, it is a variable of the curve, whereas the GAC stopping function is a constant that depends only on the image. Second, it references global information (the distribution of the image feature on the curve) rather than just pixel-wise image information. Therefore, it takes advantage of all the statistical image information that one can learn about the boundary of interest.

**Interpretation of the obtained flow:** For a clear interpretation, let us assume that $K$ is the delta function. In this case, our stopping function reduces to

$$\mathcal{G}(\mathbf{P}_\Gamma, \mathcal{M}, \mathbf{F}_\Gamma) = \mathbf{B}(\mathbf{P}_\Gamma, \mathcal{M}) - \sqrt{\frac{\mathcal{M}(\mathbf{F}_\Gamma)}{\mathbf{P}_\Gamma(\mathbf{F}_\Gamma)}}, \tag{15}$$

and has a clear interpretation. When $\Gamma$ approaches the boundary of interest, the distribution of image feature $\mathbf{P}_\Gamma$ on the curve approaches model $\mathcal{M}$. Therefore, both the global measure $\mathbf{B}(\mathbf{P}_\Gamma, \mathcal{M})$ and the pixel-wise measure $\sqrt{\frac{\mathcal{M}(\mathbf{F}_\Gamma)}{\mathbf{P}_\Gamma(\mathbf{F}_\Gamma)}}$ become very close to one. This leads to $\mathcal{G}(\mathbf{P}_\Gamma, \mathcal{M}, \mathbf{F}_\Gamma)$ approximately equal to zero, which forces the curve to stop. The refinement term attracts the curve towards pixels which increase the similarity between the distribution of image feature on the curve and model $\mathcal{M}$.

### 2.3. Level set implementation

We implemented the curve evolution equation with the level set method [15]. $\Gamma(s,t) : [0,1] \times \mathbb{R}^+ \rightarrow \Omega$ is *implicitly* represented by the zero level set of a function $\phi(\mathbf{x}, t) : \Omega \times \mathbb{R}^+ \rightarrow \mathbb{R}$, i.e., $\Gamma = \{\mathbf{x} \in \Omega \mid \phi(\mathbf{x}, t) = 0\}$. The level-set representation has well-known advantages over an explicit discretization with a finite set of points on the curve. It handles automatically topological changes, and can be effected by stable numerical schemes [15]. When $\Gamma$ evolves following

$$\frac{\partial \Gamma(s,t)}{\partial t} = V(s,t)\vec{n}(s,t), \tag{16}$$

where $V : \Omega \rightarrow \mathbb{R}$, with the convention $\phi > 0$ inside the zero level-set and $\vec{n}$ oriented outward, the corresponding level-set function $\phi$ evolves according to

$$\forall \mathbf{x} \in \Omega \ \frac{\partial \phi(\mathbf{x}, t)}{\partial t} = V(\mathbf{x}, t)\|\nabla \phi(\mathbf{x}, t)\| \tag{17}$$

In our case, the level set evolution equation corresponding to the flow we obtained is given by (17), with $V(\mathbf{x}, t)$ defined for each point $\mathbf{x} \in \Omega$ as follows

$$\begin{aligned} V(\mathbf{x}, t) &= \{\mathcal{G}(\mathbf{P}_\phi, \mathcal{M}, \mathbf{F}_\mathbf{x})\kappa_\phi(\mathbf{x}, t) \\ &- < \nabla \mathcal{G}(\mathbf{P}_\phi, \mathcal{M}, \mathbf{F}_\mathbf{x}), \frac{\nabla \phi(\mathbf{x}, t)}{\|\nabla \phi(\mathbf{x}, t)\|} >\} \end{aligned} \tag{18}$$

where stopping function $\mathcal{G}(\mathbf{P}\phi, \mathcal{M}, \mathbf{F})$ is a variable of the curve and, therefore, has to be updated during the evolution process using the distribution of image feature within a narrow band around the zero level set of $\phi$:

$$\begin{aligned} \mathbf{P}_\phi(f) &= \frac{\int_{-\delta<\phi(\mathbf{x})<\delta} K(f-\mathbf{F}(\mathbf{x}))d\mathbf{x}}{\int_{-\delta<\phi(\mathbf{x})<\delta} d\mathbf{x}} \\ \mathcal{G}(\mathbf{P}_\phi, \mathcal{M}, \mathbf{F}_\mathbf{x}) &= \mathbf{B}(\mathbf{P}_\phi, \mathcal{M}) - \sqrt{\frac{\mathcal{M}(\mathbf{F}_\mathbf{x})}{\mathbf{P}_\phi(\mathbf{F}_\mathbf{x})}} \end{aligned} \quad (19)$$

$\kappa_\phi$ is the mean curvature function of the zero level set of $\phi$ given by ($div$ is the divergence operator):

$$\kappa_\phi(\mathbf{x}, t) = div(\frac{\nabla\phi(\mathbf{x}, t)}{\|\nabla\phi(\mathbf{x}, t)\|}) \quad \forall \mathbf{x} \in \Omega \quad (20)$$

*Controlling curve evolution direction and speed:* Similar to existing edge-driven flows, the proposed flow may evolve the curve slowly and in the wrong direction when the initialization is far from the target boundary. One way to speed up curve evolution and control its direction is to add a constant velocity [8], [9]

$$\frac{\partial\phi(\mathbf{x}, t)}{\partial t} = (V(\mathbf{x}, t) + c)\|\nabla\phi(\mathbf{x}, t)\| \quad (21)$$

Note that the constant velocity can be viewed as the flow optimizing the area of the region enclosed within the curve. Coefficient $c$ can be positive or negative, depending on the initial position of the curve with respect to the target object. If the initial curve encloses the object, $c$ should be positive to speed up curve shrinking. If the initial curve is inside the target object, should be negative to speed up curve expansion. Note that, as we will show in the experiments, it is possible to choose $c = 0$ (no constant velocity), and the curve evolution still converges (in a slower motion).

*Algorithm:* The principle steps of the algorithm can be summarized as follows:

- Initialize the level set function $\phi$
- Repeat until convergence

  1. *Update distribution* $\mathbf{P}_\phi$ *and stopping function* $\mathcal{G}(\mathbf{P}_\phi, \mathcal{M}, \mathbf{F}_\mathbf{x})$ *according to* (19).

  2. *Update the level set function for each* $\mathbf{x} \in \Omega$ *according to* (21) *with* $V(\mathbf{x}, t)$ *given by* (18).

We should note that, depending on the application, the proposed flow can be used in conjunction with other region-based flows. In the following, we show experiments using solely the proposed flow to demonstrate clearly its effect.

## 3. Experiments

We applied the proposed curve evolution to the segmentation and tracking of the Left Ventricle (LV) inner (endocardium) and outer (epicardium) boundaries in 2D cardiac Magnetic Resonance (MR) images. To demonstrate explicitly the positive effect of the proposed contour-based energy, we first give two typical segmentation examples. In these examples, we run tests that show how the proposed energy can lead to improvements in accuracy over other region-based and edge-based energies. Then, we give a representative sample of the tracking results supported by quantitative performance evaluations by comparisons with manual delineations. The kernel width $h$ and narrow bound parameter $\delta$ used in estimating the feature distribution on the curve are fixed for all examples as follows: $\delta = 1, h = 1$. We used two image features, the image gradient for the tracking examples and the average intensity of pixel neighborhood for the segmentation examples.

**First typical example (segmentation of the inner boundary of the LV):** Accurate LV segmentation is acknowledged as a difficult problem [17]. Fig. 1 depicts a typical example, where the purpose is to find the boundary between the heart cavity and the background, as shown by the manual segmentation depicted by the green curve in Fig. 1 (b). This example is difficult because the background and the papillary muscles within the cavity are connected, and have the same intensity profile. Therefore, a part of the desired boundary corresponds to very small transitions of intensity (the norm of the image gradient is null or nearly null). To illustrate how the proposed energy can refine the segmentation in such examples, we compared the curve evolution methods based on the following energies:

**(1) RDM**: The region-based distribution matching energy in [3]. Optimization of this energy seeks a region, so that the distribution of image data within the region most closely matches a learned model.

**(2) RL**: The region-based likelihood energy commonly used in image segmentation [5], [12], [16]. Optimization of this energy seeks a two-region partition maximizing the conditional probability of pixel data given the learned models within the segmentation regions.

**(3) ROP**: Concatenation of RDM and the region-based overlap energy in [4], which embeds information about the overlap between the distribution of image data within the segmentation regions.

**(4) GAC**: The classical geodesic active contour energy [8] commonly used in image segmentation as an edge-based constraint, which biases the segmentation boundaries towards high gradients of image data.

**(5) EDM**: The proposed contour-based distribution matching energy (with $c = 0$, i.e., no constant velocity)

For all the energies, we used the same initialization depicted by the red curve in Fig. 1 (c), and model distributions are learned from the ground truth. We assessed the similarities between the ground truth and the segmentations obtained with both EDM, GAC, RL, RDM, and ROP using two measures, the *Dice Metric (DM)* [17] and the

*Root Mean Squared Error ($RMSE$)* with symmetric nearest neighbor correspondences [20]. The former is region-based and is given by[3] $DM = \frac{2\mathbf{A}_{am}}{\mathbf{A}_a + \mathbf{A}_m}$, with $\mathbf{A}_a$, $\mathbf{A}_m$ and $\mathbf{A}_{am}$ denoting the areas of, respectively, the automatically detected region (region inside the curve), the corresponding ground-truth region and the intersection between them. The latter is contour-based; it measures a distance between manual and automatic boundaries over $N$ number of points as follows: $RMSE = \sqrt{\frac{1}{N}\sum_{i=1}^{N}(\hat{\mathrm{x}}_i - \tilde{\mathrm{x}}_i)^2 + (\hat{\mathrm{y}}_i - \tilde{\mathrm{y}}_i)^2}$, where $(\hat{\mathrm{x}}_i,\ \hat{\mathrm{y}}_i)$ is a point on the automatic boundary and $(\tilde{\mathrm{x}}_i,\ \tilde{\mathrm{y}}_i)$ is the corresponding point on the manual boundary.

For all energies, we report $DM$ and $RMSE$ in table 1, and show the curve at convergence (red curve) superimposed to the ground-truth curve (green curve) in Fig. 1. As expected, GAC biased the curve towards high gradients of intensity (Fig. 1 (e)), thereby yielding the lowest conformity to the ground truth (highest $RMSE$ and lowest $DM$). Also, all the region-based energies did not recover accurately the target boundary due to the lack of relevant image information on the curve (Fig. 1 (f), (g), and (h)). On the contrary, with the information on the distribution of image feature within a narrow band around the curve, EDM refined accurately the result; it stopped the curve at convergence in a position very similar to the ground truth (the red curve in Fig. 1 (d)). As reported in table 1, EDM yielded a lower $RMSE$ and higher $DM$ compared to the other methods and, therefore, a higher conformity to the ground truth. This example demonstrates explicitly the usefulness of using the proposed contour-based energy in the application at hand. To illustrate quantitatively this positive effect of the proposed energy, we report in table 2 the following statistics of the segmentation obtained with RDM, ROP, and EDM:

- *Contour-based similarity measure:* The Bhattacharyya measure of similarity between the distribution of image feature within a narrow band around the curve and a model, i.e., EDM at convergence.
- *Region-based matching measure:* The Bhattacharyya measure of similarity between the distribution of image feature inside the curve at convergence and a model, i.e., RDM at convergence.
- *Region-based overlap measure:* The Bhattacharyya measure of similarity between the distribution of image feature inside and outside the curve at convergence.

With both methods, we obtained approximately the same region-based measures (refer to the first two rows in table 2), although the segmented objects are different (refer to Fig. 1 (d), (g) and (h)). On the contrary, the proposed curve evolution led to a contour-based similarity measure different from the ones obtained with RDM and ROP. These statistics show that the region-based energies in [3], [4] were not sufficient in this example, whereas the information on the distribution of image feature on the contour can limit the space of possible solutions to a curve very similar to the ground truth.

For this example, we plotted the distribution of image feature on the final curve with the model in Fig. 2 (a), and the evolution of the energy as a function of the iteration number in Fig. 2 (b). The proposed curve evolution recovered accurately the learned model, and led to a Bhattacharyya measure at convergence approximately equal to the maximum possible value ($\mathbf{B}(\mathbf{P}_\Gamma, \mathcal{M}) = 0.99 \approx 1$)).

**Second typical example (segmentation of the outer boundary of the LV):** Fig. 3 depicts detection of the outer boundary of the LV (epicardium) with the proposed curve evolution. This example is also difficult because the intensity transitions between the bottom part of the LV and the background are very small (refer to the manual delineation in Fig. 3 (a)). In this example, the model distribution is learned from a previous frame. Figs. 3 (b), (c), and (d) show, respectively, the initial curve, several intermediate evolution steps, and the final curve (red curve) superimposed to the expected delineation. The proposed energy stopped successfully the curve at the bottom part of the LV, where the background and heart myocardium are connected and have approximately the same intensity profile. In comparison to the expected delineation, it yielded a $RMSE$ equal to $1.66$ pixels and a $DM$ equal to $0.95$. The Bhattacharyya measure obtained at convergence is equal to $0.91$, whereas the initial measure is $0.68$.

**Tracking examples:** We applied the method to propagating the LV inner and outer boundaries in cardiac MR sequences, an essential but challenging task in cardiac image analysis [17], [18]. For each frame, the model distribution and initial curve are obtained from the result of the previous frame. The first frame in each sequence is segmented manually. We evaluated the tracking performance by comparisons with independent manual segmentations over $5$ sequences, each containing $10$ frames ($45$ images were automatically segmented). We give a representative sample of the results in Fig. 4 for visual inspection, and report in table 3 the statistics of the performance measures ($DM$ and $RMSE$). These indicate that the proposed energy can lead to competitive results. Note that an average $DM$ higher than $0.80$ indicates an excellent agreement with manual segmentations [19], and an average $DM$ higher than $0.90$ is, generally, difficult to obtain [18]. For instance, the study in [18] reports an average $DM$ equal to $0.81$.

## 4. Conclusion

We proposed an active curve contour-based functional which measures a similarity between the distribution of an image feature on the curve and a learned distribution model of the feature. Minimization of the functional by the Euler-

[3]Note that $DM$ is always in [0, 1], where $DM$ equal to 1 indicates a perfect match between manual and automatic segmentation.

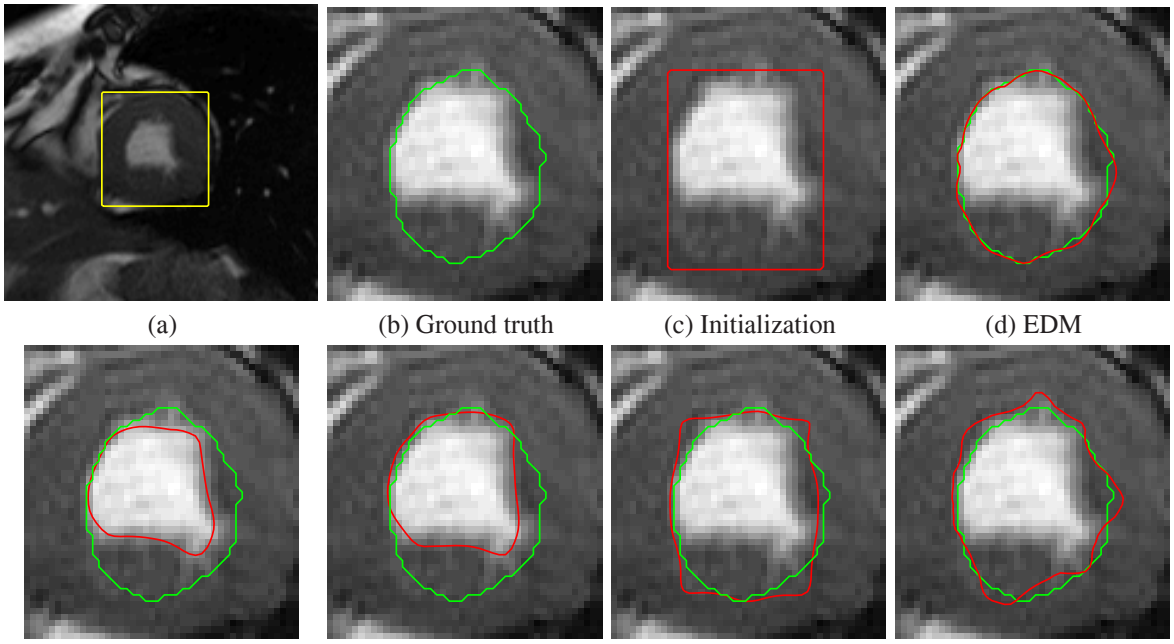

(a) (b) Ground truth (c) Initialization (d) EDM

(e) GAC (f) RL (g) RDM (h) ROP

Figure 1. Detection of the inner boundary of the LV (endocardium) in a Magnetic Resonance image. The purpose is to find the boundary between the heart cavity (foreground) and the background, as shown by the manual segmentation depicted by the green curve in (b). This example is difficult because the background and the papillary muscles within the foreground are connected, and have the same intensity profile. Therefore, a part of the desired boundary corresponds to very small transitions of intensity (the norm of the image gradient is null or nearly null). (d) depicts the curve at convergence (red curve) superimposed to the ground-truth curve with the proposed energy, i.e., with EDM. (e), (f), (g), and (h) depict the result with respectively GAC [8], RL [5], RDM [3], and ROP [4]. These energies did not recover accurately the target boundary, whereas the proposed energy refined accurately the result; it stopped the curve at a position very similar to the ground truth. For all the energies, we used the same initialization depicted by the red curve in (c), and model distributions are learned from the ground truth. Image feature for EDM: average intensity of pixel neighborhood (rectangular neighborhood of size 5 X 5 centered on the pixel). $c = 0$ (no constant velocity). The curve evolution is limited to the yellow box containing the region of interest in (a).

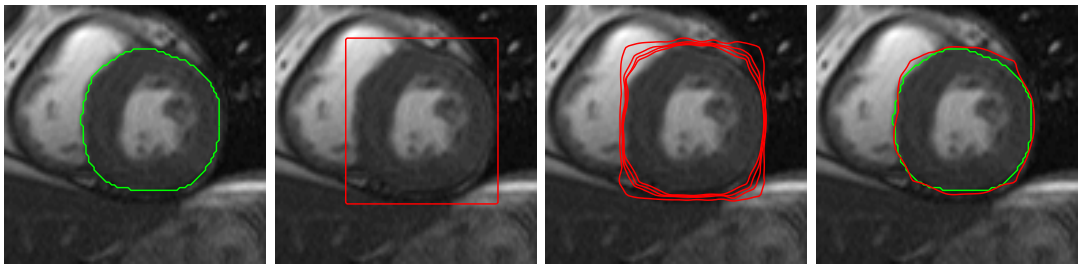

(a) Expected delineation (b) Initial curve (c) Intermediate steps (d) Final curve

Figure 3. Detection of the outer boundary of the LV (epicardium) in a MR image. This task is difficult because the intensity transitions between the bottom part of the LV and the background are very small. Model distribution $\mathcal{M}$ is learned from a previous frame. $c = 0.1$. The image feature is the average intensity of pixel neighborhood (rectangular neighborhood of size 5 X 5 centered on the pixel). (b), (c), and (d) show, respectively, the initial curve, several intermediate evolution steps, and the final curve (red curve) superimposed to the expected delineation (green curve). $RMSE = 1.66$ pixels. $DM = 0.95$. The Bhattacharyya measure obtained at convergence is equal to $0.91$, whereas the initial measure is $0.68$.

Lagrange equation resulted in a curve evolution which is viewed as a geodesic active contour with a variable stopping function. This variable stopping function depends on the distribution of image feature on the curve and, therefore, can deal with the difficult situations, where parts of the desired boundary correspond to very small transitions of image data. We gave examples which demonstrate the advantage of the proposed model over others. It would be interesting to combine the proposed functional with other region and shape constraints.

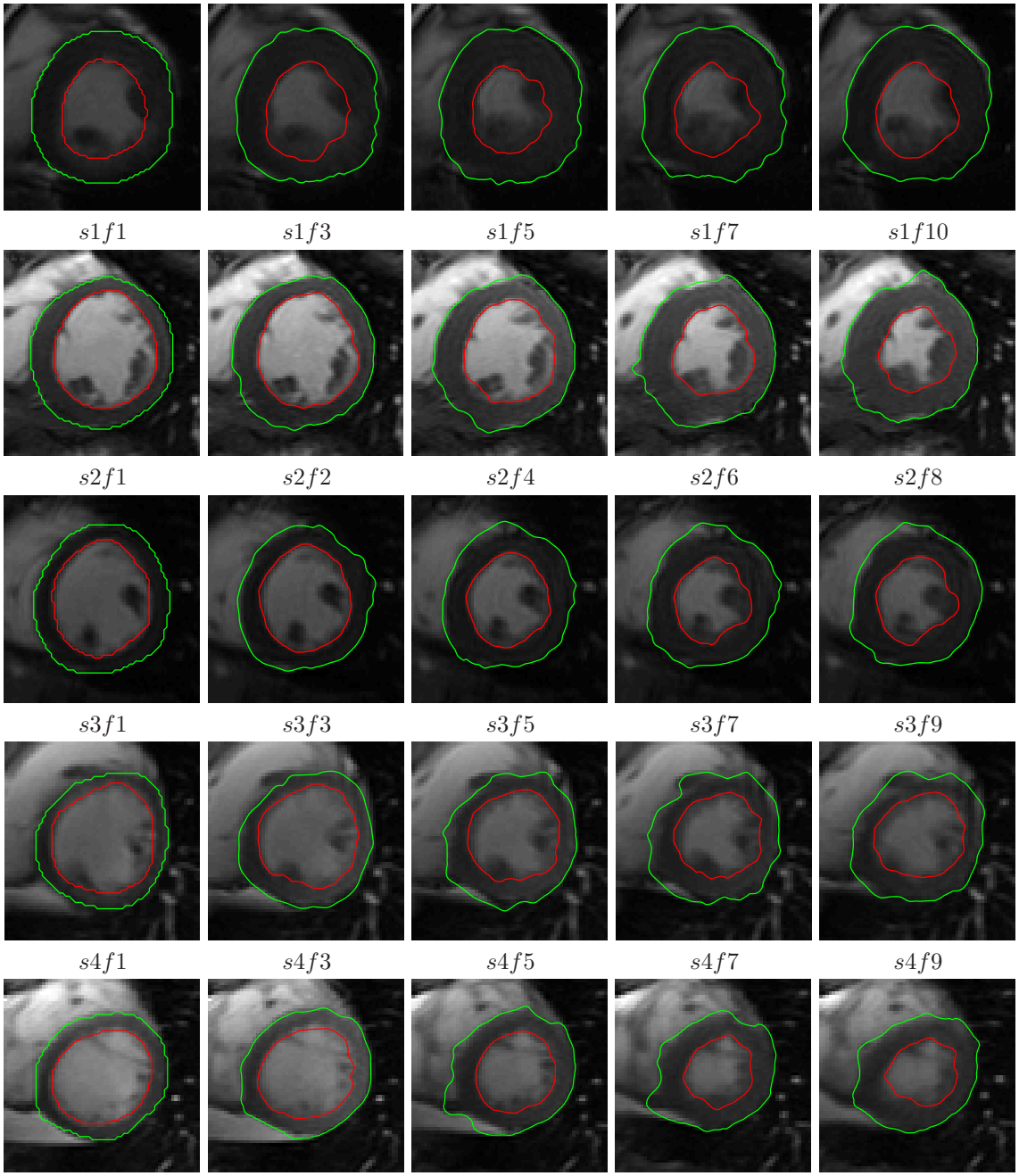


Figure 4. A representative sample of the results of tracking the inner (endocardium) and outer (epicardium) boundary of the LV in a 5 MR sequences, each containing 10 frames (systole phase of the cardiac cycle). Image feature: image gradient. $c = 0$. $sxfy$ depicts frame $y$ in sequence $x$. The method succeeded in stopping the curve at relevant positions where the transitions in intensity are very small.

## References


[1] T. F. Chan and L. A. Vese. Active Contours without Edges. *IEEE Trans. on Image Processing*, 10(2): 266-277, 2001.

[2] D. Cremers, M. Rousson, and R. Deriche. A Review of Statistical Approaches to Level Set Segmentation: Integrating Color, Texture, Motion and Shape. *International Journal of Computer Vision*, 62(3): 249-265, 2007.

[3] D. Freedman and T. Zhang. Active contours for tracking distributions. *IEEE Trans. on Image Processing*, 13(4): 518-526, 2004.

Table 1. Evaluation of $DM$ and $RMSE$ (in pixels) obtained by curve evolution with the proposed energy (EDM) and other energies. EDM yielded the lowest $RMSE$ and highest $DM$ and, therefore, the best conformity to the ground truth.

| Method | GAC | RL | RDM | ROP | EDM |
|---|---|---|---|---|---|
| $DM$ | 0.71 | 0.77 | 0.91 | 0.91 | 0.97 |
| $RMSE$ | 4.78 | 4.44 | 1.73 | 1.76 | 0.79 |

Table 2. Left ventricle inner boundary example – region-based and contour-based Bhattacharyya similarity measures obtained with RDM [3], ROP [4], and the proposed energy (EDM). The region-based measures are approximately the same with both RDM ROP, and EDM, although the segmented objects are different. On the contrary, curve evolution with EDM increased the contour-based similarity, thereby limiting the space of possible solutions to a curve very similar to the ground truth.

| Method | RDM | ROP | EDM |
|---|---|---|---|
| *Region-based matching measure* | 0.99 | 0.99 | 0.99 |
| *Region-based overlap measure* | 0.63 | 0.64 | 0.64 |
| *Contour-based matching measure* | 0.88 | 0.85 | 0.99 |

Table 3. Tracking performance evaluation of the proposed curve evolution over 5 cardiac sequences by comparisons with independent manual segmentations – means and standards deviations of $RMSE$ and $DM$

| Measure ($mean \pm std$) | $RMSE$ | $DM$ |
|---|---|---|
| *endocardium (inner)* | $1.96 \pm 0.59$ | $0.89 \pm 0.01$ |
| *epicardium (outer)* | $2.21 \pm 0.22$ | $0.93 \pm 0.01$ |

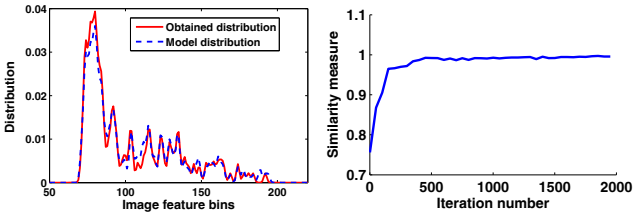


(a) (b)

Figure 2. Detection of the inner boundary of the LV – (a) distribution of image feature on the final curve and the model, (b) evolution of the energy as a function of the iteration number.


[4] I. Ben Ayed, S. Li and I. Ross. A Statistical Overlap Prior for Variational Image Segmentation. *International Journal of Computer Vision*, 85(1): 115-132, 2009

[5] M. Rousson, and D. Cremers. Efficient Kernel Density Estimation of Shape and Intensity Priors for Level Set Segmentation. *MICCAI* (2) 2005: 757-764.

[6] O. V. Michailovich, Y. Rathi, and A. Tannenbaum. Image Segmentation Using Active Contours Driven by the Bhattacharyya Gradient Flow. *IEEE Trans. on Image Processing*, 16(11): 2787-2801, 2007.

[7] X. Xie and M. Mirmehdi. MAC: Magnetostatic Active Contour Model. *IEEE Trans. Pattern Anal. Mach. Intell.*, 30(4): 632-646, 2008.

[8] V. Caselles, R. Kimmel, and G. Sapiro. Geodesic active contours. *International Journal of Computer Vision*, 22(1): 61-79, 1997.

[9] C. Li, C. Xu, C. Gui, and M. D. Fox. Level Set Evolution Without Re-initialization: A New Variational Formulation. *CVPR* 2005.

[10] N. Paragios, O. Mellina-Gottardo, and V. Ramesh. Gradient Vector Flow Fast Geometric Active Contours. *IEEE Trans. Pattern Anal. Mach. Intell.*, 26(3):402-407, 2004.

[11] S. Kichenassamy, A. Kumar, P.J. Olver, A. Tannenbaum, and A. J. Yezzi, Gradient flows and geometric active contour models. *ICCV* 1995, pp. 810-815.

[12] N. Paragios and R. Deriche. Geodesic Active Regions and Level Set Methods for Supervised Texture Segmentation. *International Journal of Computer Vision*, 46(3): 223-247, 2002.

[13] X. Bresson, S. Esedoglu, P. Vandergheynst, J. Thiran and S. Osher Fast Global Minimization of the Active Contour/Snake Model. *Journal of Mathematical Imaging and Vision*, 28(2): 151-167, 2007

[14] R. Kimmel, A. M. Bruckstein, Regularized Laplacian Zero Crossings as Optimal Edge Integrators. *International Journal of Computer Vision*, 53(3): 225-243, 2003

[15] J.Sethian. Level Set Methods and Fast Marching Methods. *Cambridge University Press*, 1999.

[16] Y. Boykov, and G. Funka-Lea. Graph Cuts and Efficient N-D Image Segmentation. *International Journal of Computer Vision*, 70(2), 109-131, 2006.

[17] I. Ben Ayed, Y. Lu, S. Li, I. Ross. Left Ventricle Tracking Using Overlap Priors. *MICCAI* (1) 2008: 1025-1033

[18] M. Lynch, O. Ghita, and P. F.Whelan. Segmentation of the Left Ventricle of the Heart in 3-D+t MRI Data Using an Optimized Nonrigid Temporal Model. *IEEE Trans. on Medical Imaging*, 27(2): 195-203, 2008.

[19] C. Pluempitiwiriyawej, J.M.F. Moura, Yi-Jen LinWu and Chien Ho. STACS: new active con- tour scheme for cardiac MR image segmentation. *IEEE Trans. on Medical Imaging*, 24 (5): 593-603, 2005.

[20] X. Papademetris, A. Sinusas, D. Dione, R. Constable, and J. Duncan. Estimation of 3-D left ventricular deformation from medical images using biomechanical models. *IEEE Trans. on Medical Imaging*, 21(7): 786-800, 2002.